NOAA Technical Memorandum NWS SR-174

# TROPICAL STORM GORDON: 72-HR RAINFALL TOTALS OVER EAST CENTRAL FLORIDA AND WSR-88D COMPARISONS

LT Barry K. Choy
Len Mazarowski
Peggy Glitto

NWSO Melbourne

Scientific Services Division
Southern Region
Fort Worth, TX

April 1996

# Tropical Storm Gordon: 72-hr Rainfall Totals Over East Central Florida and WSR-88D Comparisons

By

LT Barry K. Choy
Len Mazarowski
Peggy Glitto

NWSO Melbourne

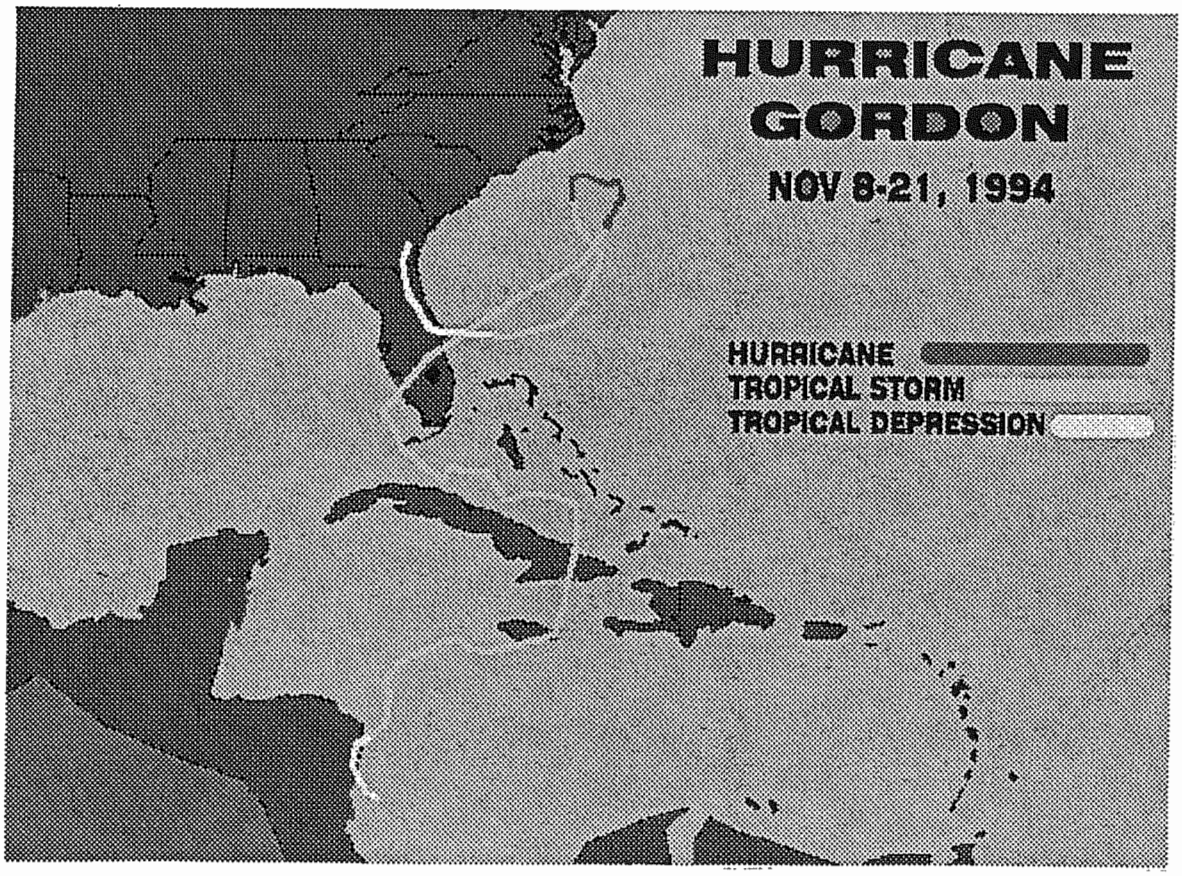

# TROPICAL STORM GORDON: 72-HR RAINFALL TOTALS OVER EAST CENTRAL FLORIDA AND WSR-88D COMPARISONS


## Abstract

Seventy-two hours of weather surveillance radar (WSR-88D) data were compared with rain gauge data during tropical storm Gordon as it impacted Central Florida on November 14-17, 1994. The WSR-88D storm total precipitation (STP) estimates were compared with 122 corresponding rain gauge readings by centering arrays of 9 and 25 STP data bins over the rain gauge locations, then performing calculations prescribed by the WSR-88D Operational Support Facility. Our results indicated the center bin STP estimates, after extreme outliers had been removed, were 46 per cent less than the corresponding 72-hr gauge totals. This difference represents an objective view of how well the radar represented rainfall without any adjustment. The WSR-88D algorithms consistently estimated rainfalls less than those recorded by the gauges, with a large dispersion between the values at the shortest and longest ranges. After adjustment was applied using the proposed correction scheme—namely using the best of nine bins with a multiplicative bias applied—the average difference decreased to 30 per cent with nearly uniform differences out to 90 nm (167 km), beyond which both the differences and dispersion increased substantially. Using the best of 25 bins with the appropriate multiplicative bias reduced the average difference to 23 per cent. Based on our analysis, it is recommended that a short-term solution would be to increase the upper reflectivity threshold to 55 dBZ and use a multiplicative bias of 1.35 to reduce the differences between the STP and surface verification during tropical systems. Future work should consider determining optimal multiplicative bias settings as a function of range from the radar.


## 1. Introduction

The WSR-88D located at the National Weather Service (NWS) office in Melbourne, Florida, has been in operation since October 1991, during which time some of the worst storms ever recorded in the area have occurred. In November 1994, Melbourne's WSR-88D captured close-up images of tropical storm Gordon. Unlike hurricane Andrew and tropical storms Alberto and Beryl, which traversed the very fringes of Melbourne's WSR-88D area of coverage, Gordon passed directly over Central Florida. The heavy rains and subsequent flooding associated with T. S. Gordon were widespread and damaging for the residents of Central Florida.

Post-analyses of previous heavy rain events suggest that the accuracy of the WSR-88D storm total precipitation (STP) algorithm varies, depending on the type of weather system, source of rain (stratiform or convective), and time of year. Sporadic and erroneous surface data, poor graphical STP resolution (as displayed on screen), and data time continuity problems made these past analyses difficult to perform and yielded primarily subjective results in the Florida area. Many of these problems were recently resolved, making systematic rainfall comparison between numerous surface rain gauges and the WSR-88D possible in a reasonable amount of time and with improved resolution.

In addition to data from numerous NWS and cooperative observer sites, the NWS Weather Office at Melbourne receives rainfall data from the St. Johns River Water Management District network of gauges in support of NASA's Tropical Rainfall Measuring Mission (TRMM). Systematic rainfall comparison procedures developed by the WSR-88D Operational Support Facility (OSF) Applications Branch were made available to Melbourne a few weeks before tropical storm Gordon moved over Central Florida (Kelly 1994). Subsequently, it was possible to compare the

data from 122 rain gauges within the 124 nm (230 km) Melbourne WSR-88D umbrella of coverage to the STP estimates for this tropical system.

Our intent was to evaluate the radar's performance in a significant tropical rain event. This is the first of many studies needed to help determine which meteorological situations result in significant radar-gauge rainfall differences in Central Florida. We expect that the results of studies such as this will make it possible to properly minimize these radar-gauge differences through the use of appropriate site- and situation-adaptable parameters.

A brief background on the WSR-88D, information on the rain gauge networks in the Central Florida area, and a detailed analysis of gauge/WSR-88D comparisons for 72-hr of T. S. Gordon's path across Central Florida were compiled and are presented in the following sections.

## 2. Background

The Melbourne WSR-88D Radar Data Acquisition (RDA) unit and Radar Products Generator (RPG) are located along the east Central Florida coast approximately 20 nm (37 km) south of Cape Canaveral (Fig. 1). Associated Principle User Positions are located at Melbourne (collocated with the RDA and RPG), Patrick Air Force Base, and the Kennedy Space Center's Range Operations Control Center. WSR-88D radars overlapping Melbourne's umbrella of coverage are located in Ruskin (near Tampa) to the west and Miami to the south. All of these WSR-88D radars currently use the same rainfall processing techniques.

## 3. WSR-88D Precipitation Processing

The WSR-88D uses a complex system of algorithms to estimate rainfall over its 124 nm (230 km) umbrella of coverage. Within this precipitation processing system, a hybrid scan technique provides continuity between base reflectivity sample volumes, which are used to compute rainfall rates (Fig. 2). The hybrid scan technique uses reflectivities from several elevation slices depending on the range from the RDA. A process called bi-scan maximization is used beyond 27 nm to determine which of the lowest two elevation slices is best. This ensures that all sample volumes are taken from nearly the same altitude, approximately 3000 ft (1 km) and minimizes errors due to ground clutter contamination (*Federal Meteorological Handbook No. 11*).

In bi-scan maximization (used at distances beyond 27 nm from the RDA), the maximum reflectivity value is chosen from the 0.5° and 1.5° slices. If ground clutter is detected, the sample volume from the 1.5° elevation angle is used, thus reducing the likelihood of contamination due to the ground clutter. However, bi-scan maximization may yield precipitation estimates that are too large due to the presence of bright bands or virga. An example of bright band contamination seen over Central Florida during a moderate rainfall event in December 1994 is presented in Fig. 3 and Plate 1.

The precipitation preprocessing algorithm computes rainfall rates (R) using the formula $Z=300R^{1.4}$ where Z is the base reflectivity from the sectorized hybrid scan. The output is a rainfall rate for each sample volume. Since the sample volume size increases with increasing range from the radar, the algorithm adjusts the sample volumes to make them nearly uniform and also applies time continuity and range corrections. The output from the precipitation rate algorithm is

corrected rainfall rates for each 1° x 1.1 nm (2.0 km) sample volume for the graphical products and for each 2.2 nm x 2.2 nm (4.1 km) sample volume for the digital product.

The precipitation accumulation algorithm uses the computed rainfall rates to compute totals of one-hour precipitation (total from past hour, updated each volume scan), three-hour precipitation (total for past three hours, updated on the hour), and storm total precipitation (running total of accumulated precipitation since the STP was last reset). Although not currently implemented, a precipitation adjustment algorithm will eventually determine hourly rainfall accumulations for each graphical and digital sample volume. A gauge-to-radar bias will be calculated and the correction applied. The output will be an adjusted scan-to-scan and hourly rainfall accumulation for each sample volume.

Errors in rainfall rate and rainfall accumulation computations may stem from gaps between volume scans or missing volume scans. (The rainfall algorithms adjust for missing data by using data on either side of the missing data.) Errors may also result from hardware calibration errors, anomalous propagation, and signal attenuation due to a wet radome. Site adaptable thresholds are set to minimize the effect of spurious weak reflectivity returns and overestimation of rainfall due to hail contamination. At present, the WSR-88D uses thresholds of 18 and 53 DBZ. Rainfall is not computed from reflectivity values below 18 DBZ, and all reflectivities greater than 53 DBZ are truncated to reflect rainfall at the rate corresponding to that value. The 53 DBZ threshold and the current Z-R relation limit the maximum computed rainfall rate to 4.09 in/hr (103.8 mm/hr). This may be a source of the underestimation error in tropical environments where rainfall rates in excess of this limit are often observed without hail being present (Fig. 4).

Additionally, the Z-R relationship may not be representative of the predominant type or intensity of precipitation for every weather situation. Errors due to evaporation of rain below the sampling altitude or the transport of precipitation by strong horizontal winds may also occur.

Future plans call for the implementation of a Kalman filter to compute a multiplicative bias between real-time rain gauge measurements from the gauge data acquisition system and the radar precipitation estimates from the best of the nine bins (centered over the gauge). The bias would be independently calculated each hour using the mean and standard deviation of each gauge/radar pair. A minimum of five sets of gage/radar pairs within the radar cylinder of coverage would be needed for precipitation bias to be computed. Gauge/radar differences less than 0.024 in (0.061 mm), or with normalized differences greater than two standard deviations, would be excluded.

## 4. Rain Gauge Network

A total of over 200 surface point rainfall data sources are available within a 124 nm (230 km) radius of the NWSO Melbourne WSR-88D. Of these, 122 gauges reported useful time-matched data for the 72-hr of T. S. Gordon's influence on Central Florida.

The St. Johns River Water Management District operates a tipping bucket rain gauge network over much of Central Florida. Each gauge in the network is connected to a data collection and storage facility in Palatka, Florida, with remote access via computer and modem. A data base of gauges can be queried as far back as one year, with a temporal resolution as fine as one minute. In support of the WSR-88D evaluation as part of NASA TRMM, Melbourne was

provided with computer and communications equipment which allows direct access to many of the St. Johns River basin gauges and access to entire network via the computer in Palatka.

In addition to the data from the St. Johns River Water Management District network, data were available from 31 gauges owned and maintained by the United States Geological Survey. These are tipping buckets with one-hundredth inch increment accumulators. Data were also available from 47 NWS and cooperative observer stations. Most of these sites use standard 8-in (203.2 mm) rain gauges, with redundant tipping buckets at NWS installations. Data were also available from an optical rain gauge located on a weather data buoy about 20 nm (37 km) from Cape Canaveral (Fig 1).

## 5. Methods

Data from the 122 rain gauges were compared to the corresponding WSR-88D STP values for the 72-hr period 1200 UTC November 14 to 1200 UTC November 17, 1994. To maintain time continuity between the data sources, the STP product was reset at 1211 UTC November 14, prior to any heavy rainfall associated with T. S. Gordon. The WSR-88D HYPROD.DAT file was copied to a data tape at the RPG on November 17 at 1223 UTC. Thus, nearly 72 hours of radar computed rainfall accumulations were collected.

The WSR-88D Operational Support Facility systematically compared the STP estimates with the gauge totals to evaluate how well the WSR-88D estimated total rainfall during this tropical rainfall event (Kelly 1994). Since it was unlikely that any gauge was directly under an STP bin, the gauge data were compared to an array of nine bins approximately centered over each gauge.

The gauge total was compared with several radar estimates within the nine bin array. The first, called *center*, compared the gauge total with the radar estimate for the bin most nearly over the gauge. The second, called *maximum,* was a comparison between the gauge total and the largest of the nine radar estimates. The third, called *minimum*, was similar to the second, except the smallest of the radar estimates was compared to the gauge total. The fourth, called *best bin*, compared the gauge total to the radar estimate with the least difference from the gauge total. If the gauge total fell between the minimum and maximum values within the bin array, the best bin was the gauge total. The last, called *average*, compared the gauge total to the average value of the nine radar bins.

The center, best fit, maximum, minimum, and average of the bins were computed for each gauge. Additionally, a 25 bin analysis was performed to determine if a larger array would yield more accurate results (Fig. 5).

Mean radar bias, relative dispersion (coefficient of variation), and average differences were calculated as prescribed by the OSF (Fig. 6). These analyses were developed to simulate the WSR-88D's processing of radar/gauge data and to standardize the output the OSF received from participating offices.

In preliminary computations (Fig. 7), larger radar-gauge differences were noted at the shortest (within 27 nm; 50 km) and longest (beyond 90 nm; 167 km) ranges from the radar, as compared with the intermediate range (27-90 nm; 50-167 km). To achieve a more representative multiplicative bias over the entire radar coverage area, an additional set of statistical analyses

were performed separately on these three range categories. Average radar-gauge differences were computed for each range category, omitting G/R values that were two or more standard deviations from the mean. The revised bias was applied in ( Fig. 6, Equation 5), and the average difference was recomputed.

## 6. Results

Within the 124 nm (230 km) radar coverage umbrella, accumulated rainfall totals for the 72-hr period ranged from near zero to approximately 16 in (406 mm), with the majority of gauges recording less than 10 in (254 mm) of rainfall (Fig. 8). However, based on radar STP estimates (Plate 2) and the computed mean bias, areas offshore and isolated areas inland probably received more than 16 in (406 mm) of rain.

The results of the analysis over the entire range 0 - 124 nm (0 - 230 km) indicated the center bin STP estimates, after extreme outliers had been removed, were 46 per cent less than the corresponding 72-hr gauge totals (Table 1). This difference represents an objective view of how well the radar represented rainfall without any adjustment. The WSR-88D algorithms consistently estimated rainfalls less than those recorded by the gauges, with a large dispersion between the values at the shortest and longest ranges. After adjustment was applied using the proposed correction scheme—namely using the best of nine bins with the multiplicative bias applied—the average difference decreased to 30 per cent (Table 1), with nearly uniform differences out to 90 nm (167 km), beyond which both the differences and dispersion increased substantially. Using the best of 25 bins with multiplicative bias reduced the average difference to 23 per cent.

Table 1. Results of nine- and 25-bin analyses for all ranges with outliers removed.

| PARAMETER | Without Adjustment (Center Bin) | With Adjustment (Best of Nine Bins) | With Adjustment (Best of 25 Bins) |
|---|---|---|---|
| Mean Radar Bias (Eq. 1) | 1.65 | 1.44 | 1.35 |
| Mean Radar Bias (Eq. 2) | 2.05 | 1.57 | 1.36 |
| Relative Dispersion (Eq. 3) | 71% | 41% | 26% |
| Average Difference (Eq. 4) | 46% | 35% | 26% |
| Average Adjusted Difference (Eq. 5) | 49% | 30% | 23% |

Large differences between radar and gauge measurements and a greater relative dispersion within the 27 nm (50 km) range and beyond 90 nm (173 nm) were noted when uncorrected radar-gauge differences were plotted (Fig. 9). The data were therefore stratified into three range classes, based on the dispersion of data points within each range class. The range classes were analyzed separately in an attempt to develop a better correction over the entire range by applying a range specific multiplicative bias to each range class.

Within the shortest range class (0-27 nm) the average difference, using the center bin, was 42 per cent (Table 2). Applying the proposed corrective technique significantly reduced the difference

to 17 per cent. The relative dispersion was also significantly reduced. Using a 25-bin array resulted in a slight improvement over the nine-bin array.

Table 2. Results of nine- and 25-bin analyses for shortest range (0 - 27 nm)

| PARAMETER | Without Adjustment (Center Bin) | With Adjustment (Best of Nine Bins) | With Adjustment (Best of 25 Bins) |
|---|---|---|---|
| Mean Radar Bias (Eq. 1) | 1.79 | 1.47 | 1.39 |
| Mean Radar Bias (Eq. 2) | 2.04 | 1.43 | 1.33 |
| Relative Dispersion (Eq. 3) | 65% | 23% | 17% |
| Average Difference (EQ. 4) | 42% | 30% | 24% |
| Average Adjusted Difference (Eq. 5) | 46% | 17% | 13% |

The average uncorrected difference of the intermediate range class (27-90 nm) was 34 per cent, decreasing to 15 per cent after a multiplicative bias of 1.32 was applied (Table 3). The relative dispersion also decreased. Using a 25-bin array resulted in only a minor improvement over the nine-bin array.

Table 3. Results of nine- and 25-bin analyses for intermediate range (27 to 90 nm)

| PARAMETER | Without Adjustment (Center Bin) | With Adjustment (Best of Nine Bins) | With Adjustment (Best of 25 Bins) |
|---|---|---|---|
| Mean Radar Bias (Eq. 1) | 1.45 | 1.28 | 1.19 |
| Mean Radar Bias (Eq. 2) | 1.53 | 1.32 | 1.21 |
| Relative Dispersion (Eq. 3) | 24% | 20% | 16% |
| Average Difference (Eq. 4) | 34% | 23% | 16% |
| Average Adjusted Difference (Eq. 5) | 16% | 15% | 14% |

The average uncorrected difference for the longest range class (90-124 km) was 54 per cent, decreasing sightly to 49 per cent after the multiplicative bias of 2.33 was applied (Table 4). The improvement was primarily due to the large relative dispersion (coefficient of variation) over that range. For this range class, the use of a 25-bin array resulted in a substantial improvement over the nine-bin array. Average differences decreased from 49 per cent to 25 per cent, with relative dispersion decreasing from 44 per cent to 36 per cent. It is important to note that, within the 25-bin array, the best bin becomes the gauge total if the gauge total falls between the STP min and max bin within the array. The probability of this occurring over a 25-bin array is far greater than that for the 9-bin (see Appendices A and B for complete analysis results).

Table 4. Results of nine- and 25-bin analyses for longest range (90 to 124 nm)

| PARAMETER | Without Adjustment (Center Bin) | With Adjustment (Best of Nine Bins) | With Adjustment (Best of 25 Bins) |
|---|---|---|---|
| Mean Radar Bias (Eq. 1) | 1.93 | 1.77 | 1.64 |
| Mean Radar Bias (Eq. 2) | 2.79 | 2.33 | 1.71 |
| Relative Dispersion (Eq. 3) | 80% | 69% | 32% |
| Average Difference (Eq. 4) | 54% | 44% | 36% |
| Average Adjusted Difference (Eq. 5) | 53% | 49% | 25% |

## 7. Summary

Comparing the STP bins centered over the gauges for the entire range yielded a 46 per cent average radar-gauge difference when no corrective measures were applied. When the proposed corrective technique was employed (best bin of the surrounding nine-bin array, with a multiplicative adjustment) the average difference was reduced to 30 per cent. The application of this technique significantly improved the radar estimated rainfall at the intermediate range (90-124 nm; 167-230 km). Within 90 nm, radar estimates were over-increased to where most of the radar estimates were in excess of gauge amounts. This over-estimation was due to the multiplicative bias being skewed to represent most accurately values where most of the data points occurred, namely from 90 nm to 124 nm. To further reduce errors within 90 nm, a multiplicative bias of 1.43, 1.32, and 2.33 was applied separately to the range sets 0-27 nm (0-50 km), 27-90 nm (50-167 km), and 90-124 nm (167-230 km), respectively. This improved the radar estimates, particularly within 90 nm.

## 8. Discussion

It is important to note that these post analyses do not necessarily reflect results that might be achieved in real-time. Data from 122 gauges were used in these analyses, whereas in real-time we might expect to obtain only a small fraction of these. Additionally, in the real-time adjustments the multiplicative bias and corrections would be each hour, while only storm totals were used in this study.

Post analysis of the T. S. Gordon case suggests that using the prescribed corrective technique would produce an unacceptably large average difference between the radar precipitation estimate and measured gauge totals (30 per cent). By stratifying the data into three range categories this error was reduced to about one-half of that for the entire range (or 15 per cent). Using the range categories and a 25 bin array yielded even better results overall, and within each range category.

For this case, applying a multiplicative bias within 90 nm (167 km) yielded rainfall estimates which were about 85 per cent of the actual ground truth for both the nine or 25 bin analyses. Beyond 90 nm, the best of 25 bin analysis yielded an AD = 25 per cent. Thus, the corrected radar estimate was 75 per cent of ground truth. It is important to note, however, that the relative dispersion beyond 90 nm was high compared with those for the closer range categories, and it may not be reasonable to consider any estimates beyond 90 nm (167 km).

Sources of error span a realm of possibilities, with several sources contributing to the final difference between radar estimated rainfall and ground truth. It is not an easy task to properly adjust the radar estimates without first understanding where the major error sources lie, and determining whether these error sources are the same for all weather situations. For instance, it has been noticed (Wolff 1994) that significant (30 db at times) errors exist due to the hybrid scan construction, especially between elevation slices close to the RDA. This may be a major contributor to the errors noticed within the 27 nm (50 km) range for this case. Beyond this range, perhaps effects below the beam contributed to a large portion of the difference. Our point is, a single multiplicative bias cannot be expected to reasonably correct for errors resulting in varying degrees from several sources, especially when they are range-dependent.

Although adjusting the Z-R relation and altering reflectivity thresholds may improve the overall rain estimation, there still may be significant differences between radar estimates and actual rainfalls. More complex processing would be needed to reduce errors at all ranges and for all situations. This processing might have to account for the fraction of precipitation being generated by different processes. In extratropical rainfall the current approach probably works well, because the current Z-R relation works well for deep convection (thunderstorms). In tropical rainfall the distribution of cell types and the rain formation processes vary greatly from those in extratropical systems. While the current Z-R relation may be applicable to the most intense cells within a tropical system, these cells may represent only a small fraction of the rainfall. Low topped cells producing heavy precipitation may be the largest contributor. The precipitation from such cells will be severely underestimated due to below-beam effects. The problem is compounded when fraction and types of rainfall change as systems evolve.

For maritime precipitation it has been noted that heavier rainfall is indicated offshore than onshore much of the time, with the transition being extremely pronounced (Plate 2). Although not a major problem for the general public, since rainfall occurring over the water does not contribute to surface runoff, it may be significant for island locations. For tropical rainfall over water, the Z-R relationship currently employed with the WSR-88D may be a reasonable estimator, once reflectivity upper thresholds are adjusted (Fig. 4). In the long term, our hope is that accurate corrections could be applied for all situations using complex processing techniques.

The long-term approach to rainfall correction might use an artificial intelligence scheme that can recognize various weather systems (by model and/or environmental data input) and the percentage distribution of rainfall realized at the surface due to various processes. With such a scheme the radar could recognize those areas that were convective, stratiform, and/or low-topped precipitation, and recognize that a tropical system may have a larger proportion of precipitation with higher reflectivities below the beam. Appropriate corrective measures (change Z-R, thresholds, etc.) could then be applied differently to changing predominant precipitation areas and various weather systems automatically, instead of entire ranges all the time. Perhaps this is an ambitious endeavor at this point, but it may soon be obtainable with technological advances.

In the near future various aspects of cloud physical processes need to be addressed in more detail by the scientific community. For instance, the distribution of condensation nuclei varies from marine environments to continental areas. Large condensation nuclei are more prominent in marine environments due to the higher concentration of salt particles within the aerosol; whereas over the continent dust, pollen, and other nuclei are more numerous. One implication of salt

nuclei is the particles are soluble. Water condensation on the surface of a saline drop can continue to take place at lower vapor pressures than fresh water drops (non-soluble nuclei). Thus, where fresh water drops may evaporate as they fall, decreasing in size, solution drops may actually achieve equilibrium or continue growth as they fall (Wallace and Hobbs 1977). In the latter case, one would expect the largest drops, and subsequently the highest reflectivities, to be at lower altitudes as drops grow and coalescence occurs.

The observed vertical reflectivity distribution in tropical rainfall also indicates the highest reflectivities at low levels (Fig. 11). In the 27-90 nm (50-167 km) range, the beam center for the 0.5° elevation slice samples ranges from 2000 ft (610 m) to near 11,000 ft (3354 m), and higher beyond 90 nm, under standard refractive conditions. Thus, sampling largely occurs at elevations where reflectivity is a fraction of that near the surface, and errors seem to support this as well.

Operationally, a search for short-term approaches which would aim at improving rainfall estimation through the use of the current system may be a major goal. For tropical systems, this may be as simple as increasing estimated rainfall by applying uniform multiplicative bias of 1.35 to the area within 90 nm (167 km) and omitting anything beyond 90 nm. It may be possible to improve results within 27 nm (50 km) by changing the hybrid scan construction for tropical systems by using lower elevation angles within 27 nm. Various Z-R relations and associated thresholds should be examined for different systems; however, current Z-R relations derived from tropical rainfall data (Fig. 12) indicate very little variation, and most certainly would not account for the magnitude of differences observed in the T. S. Gordon. NWS offices can make a large contribution to improving the long-term corrective processes by collecting data and performing analyses similar to what was done for this case.

Future work in Florida should aim to provide short-term solutions to obtaining good rainfall estimates from the WSR-88D. Rainfall events should be analyzed from both a meteorological and hydrological perspective, possibly identifying and allowing for the adjustment of thresholds, or possibly by adjusting Z-R relations for events. Temperature, moisture, and instability should all be evaluated (at many levels) to identify similarities and differences in events. Rainfall comparisons for similar events (i.e., tropical systems) should be compared and event specific adaptable parameters identified. Additionally, differences between overlapping WSR-88Ds should be identified through coordinated rainfall comparisons with the Tampa and Miami radars. For tropical systems, or precipitation generated by tropical processes, a manually employed multiplicative bias of 1.35 might reduce errors significantly and should be pursued.

Throughout modernization the importance of real-time measurement cannot be overstressed. If accurate remote rainfall estimation is to become a reality, the integrity of the rain gauge network must be maintained.

## 9. Conclusions

The WSR-88D at the Melbourne NWSO significantly underestimated rainfall during T. S. Gordon, with an average difference of 35 per cent using the best match of nine bins over the entire range. Post-analyses indicated that, on average, using the prescribed corrective technique would yield an average difference of 30 per cent for the same time period and area even after the multiplicative bias was applied. A 30 per cent difference may be insignificant in low rainfall

events; but for rainfall totals as large as 16 in (406 mm), a 5 in (127 mm) underestimation would occur. Applying the same corrective technique and separating the area into three range categories reduced the errors significantly out to 90 nm (167 km). Using a 25 bin analysis with the three range categories further reduced the errors. These results indicate that further study is warranted in order to determine the most effective and efficient technique for adjusting radar-derived rainfall estimates using observed gauge totals. With its dense network of rain gauges and high frequency of tropical convective systems, Florida remains an excellent area for research on tropical rainfalls.

**Acknowledgements.** The authors greatly appreciate the dedicated efforts of D. Scott Kelly (OSF), who processed the HYPROD.DAT files and provided the gauge-centered STP output, and Ian Palao (National Data Buoy Center), who provided the optical rain gauge data from buoy 41009. Special thanks to all the reviewers who provided comments and suggestions. Thanks also to Bernard N. Meisner and Marsha Spencer (NWS Southern Region, Scientific Services Division) for their editorial assistance.

## REFERENCES

Choy, B. K., M. T. Trexler, 1994: Using a fast boat to investigate offshore weather features in conjunction with WSR-88D observations. *NOAA Tech. Memo.* NWS SR-159, 25 pp.

Kelly, D.S., 1994: Procedures for forecast offices to perform gage-radar comparisons. WSR-88D user's conference presentation (publication pending)., 8 pp.

*Federal Meteorological Handbook No. 11 - Part C*: WSR-88D Products and Algorithms. Washington, D. C., 1991.

Ramana Murty, Bh. V. and S. C. Gupta, 1959: Precipitation characteristics based on raindrop sizemeasurements at Delhi and Khandala during southwest monsoon. *J. Sci. Industrial Res.*, New Delhi, 18A, 352-371.

Wallace, J. M. and P. V. Hobbs, 1977: *Atmospheric Science an Introductory Survey*. Academic Press, New York, NY, pp. 143 - 209.

Wexler, R., 1948: Rain intensities by radar. *J. Meteor.*, 5, 171-173.

Wolff, D. B., 1994: Issues noted regarding the Melbourne, Florida WSR-88D radar calibration. Internal correspondence, 5 pp.

# Rain Gauges Used (within 124 nm of the MLB WSR-88D)

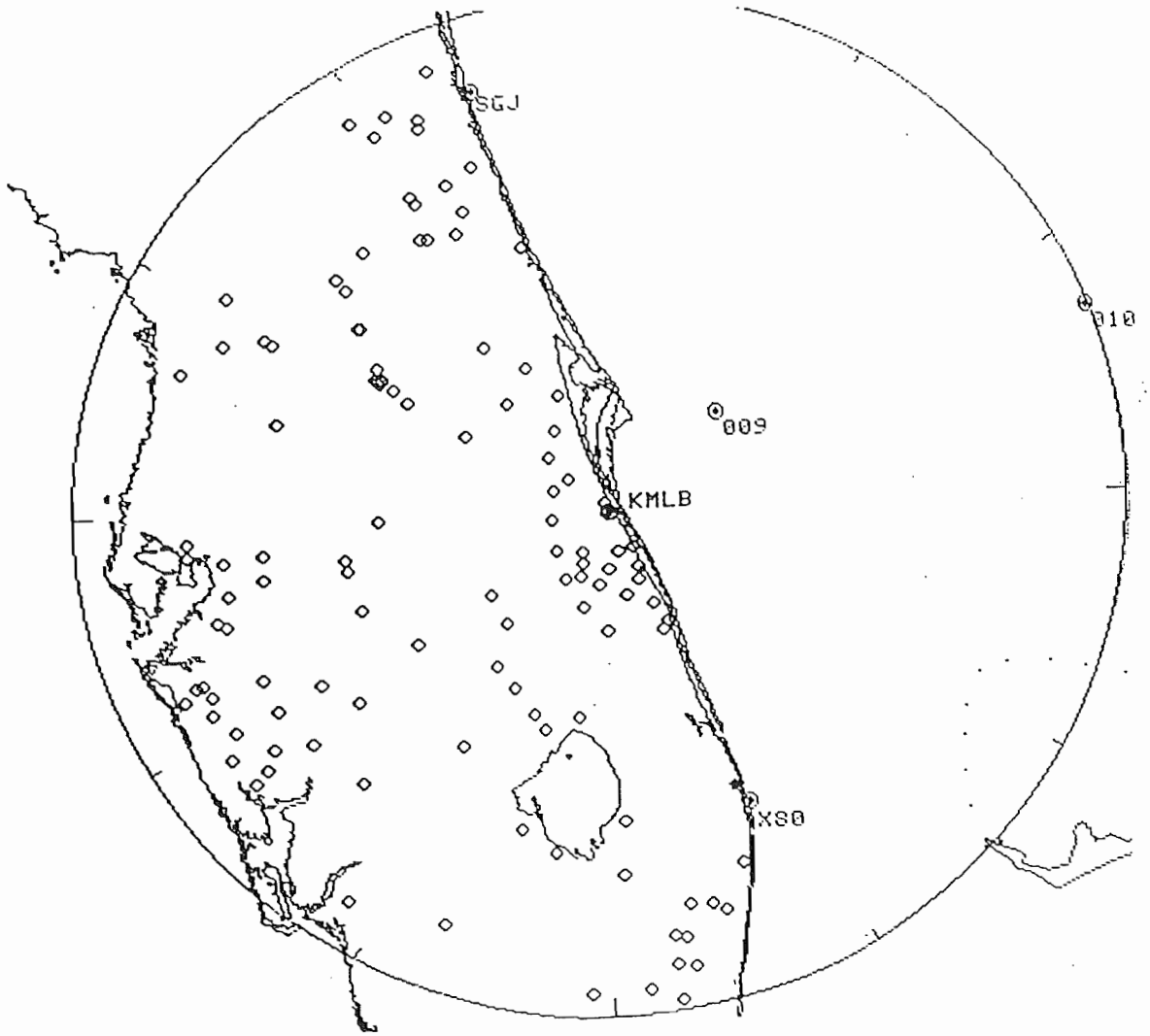


Figure 1 - Map of the central Florida area. The range ring defines the 124 nm (230 km) area of WSR-88D rainfall estimation within which rain gauges are also indicated (◇).

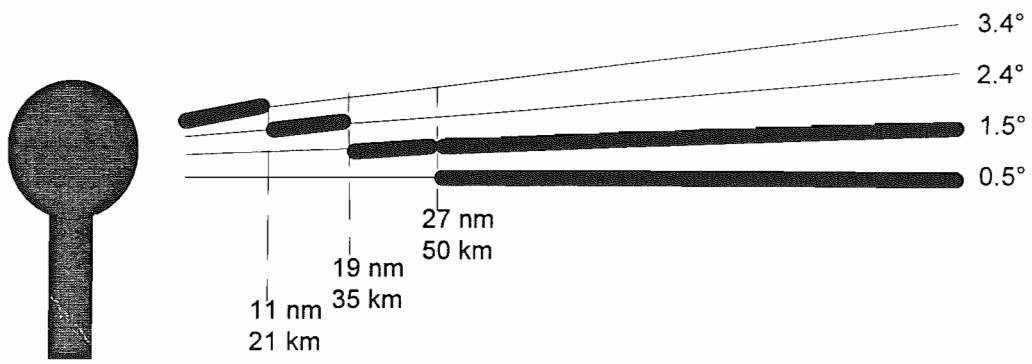


Figure 2 - The WSR-88D uses higher elevation angles close in and lower angles as distance increases from the radar to maintain nearly uniform sampling height above the surface (under standard refraction conditions). This graphical depiction illustrates the elevation angles used at the various distances from the RDA (Radar Data Acquisition unit).

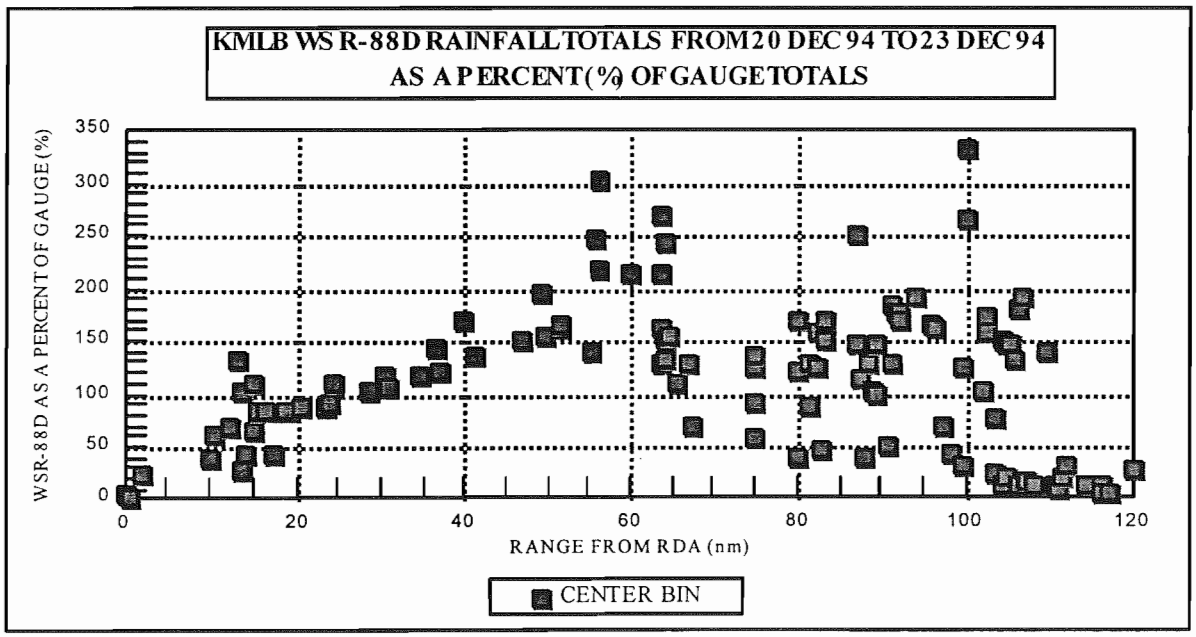


Figure 3 - Radar estimated rainfall as a percent of actual measured rainfall during a winter rain event. Note bright band contamination (radar overestimation) between about 35 nm and 70 nm.

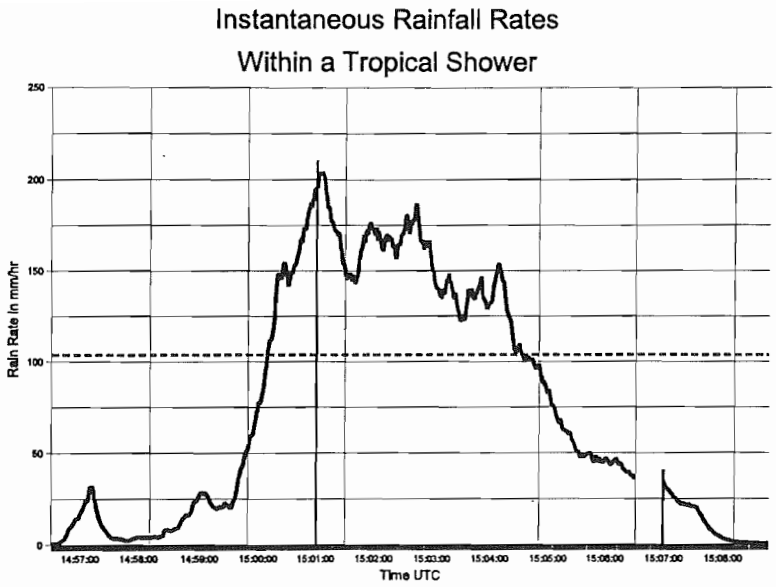


Figure 4 - During the SWIFT BOAT '94 project (Choy and Trexler, 1994) rainfall was measured in convective cells offshore using an optical rain gauge (provided by NASA TRMM) mounted on a fast boat. Due to poor reflectivity resolution as displayed by the WSR-88D, which is 5 dBZ (i.e. 50 - 54 dBZ ), rainfall rate was manually computed for the lower and upper reflectivity values for the sample volume directly over the vessel (fitted with the gauge); as a convective cell passed directly over the vessel. The average of these two rates (vertical lines) indicated that if a upper threshold was not implemented (dashed line) the radar may have computed the rates near correctly. The WSR-88D sample volume times were 15:01 and 15:07 UTC.

**0101 : AZ=181.6 Range= 52.7 km**

| Km\Az | 179.5 | 180.5 | 181.5 | 182.5 | 183.5 |
|---|---|---|---|---|---|
| 57: | 4.71 | 4.73 | 4.79 | 4.88 | 4.68 |
| 55: | 4.76 | 4.83 | 5.19 | 4.66 | 4.73 |
| 53: | 5.53 | 5.22 | 5.38 | 5.26 | 5.67 |
| 51: | 5.52 | 5.73 | 5.38 | 5.37 | 5.54 |
| 49: | 5.04 | 4.94 | 4.35 | 4.55 | 4.48 |

**MAX: 5.73 MIN: 4.66 AVG: 5.22**

Figure.5 - The STP calculations for 25-bins centered over gauge 0101 with MAX, MIN, and AVG listed for the 9 center bins. The azimuth (top) and range (left) of each bin define its location with respect to the RDA (Melbourne WSR-88D).

$$\textit{Mean Radar Bias}\ (1) = \frac{\sum_{i=1}^{N} G_i}{\sum_{i=1}^{N} R_i} \qquad \textit{Mean Radar Bias}\ (2) = \frac{1}{N}\sum_{i=1}^{N} \frac{G_i}{R_i}$$

$$\textit{Relative Dispersion}\ (3) = \frac{\sigma\,[G/R]}{\overline{G/R}} * 100\ \%$$

$$\textit{Avg. Diff.}\ (4) = \frac{1}{N}\sum_{i=1}^{N} \left| \frac{(G_i - R_i)}{G_i} \right| * 100\ \% \qquad \textit{Avg. Diff.}\ (5) = \frac{1}{N}\sum_{i=1}^{N} \left| \frac{(G_i - (\overline{G/R})\,R_i}{G_i} \right| * 100\ \%$$

Figure 6 - In all equations ($G$) is the gauge total and ($R$) is the corresponding radar STP total. The radar bias is calculated twice (top left) first with a weight assigned to the observations (proportional to the gage amount) and second (top right) with all comparisons receiving equal weight. Average Difference is calculated (bottom left) and then recalculated (bottom right) applying the mean radar bias.

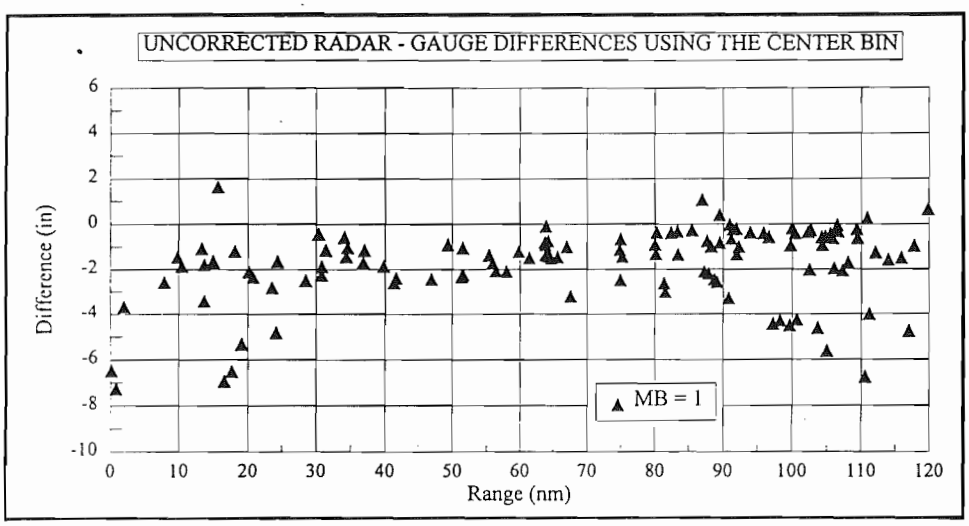


Figure 7 - Center bin radar estimated values plotted as a percent of the gauge totals for all gauges.

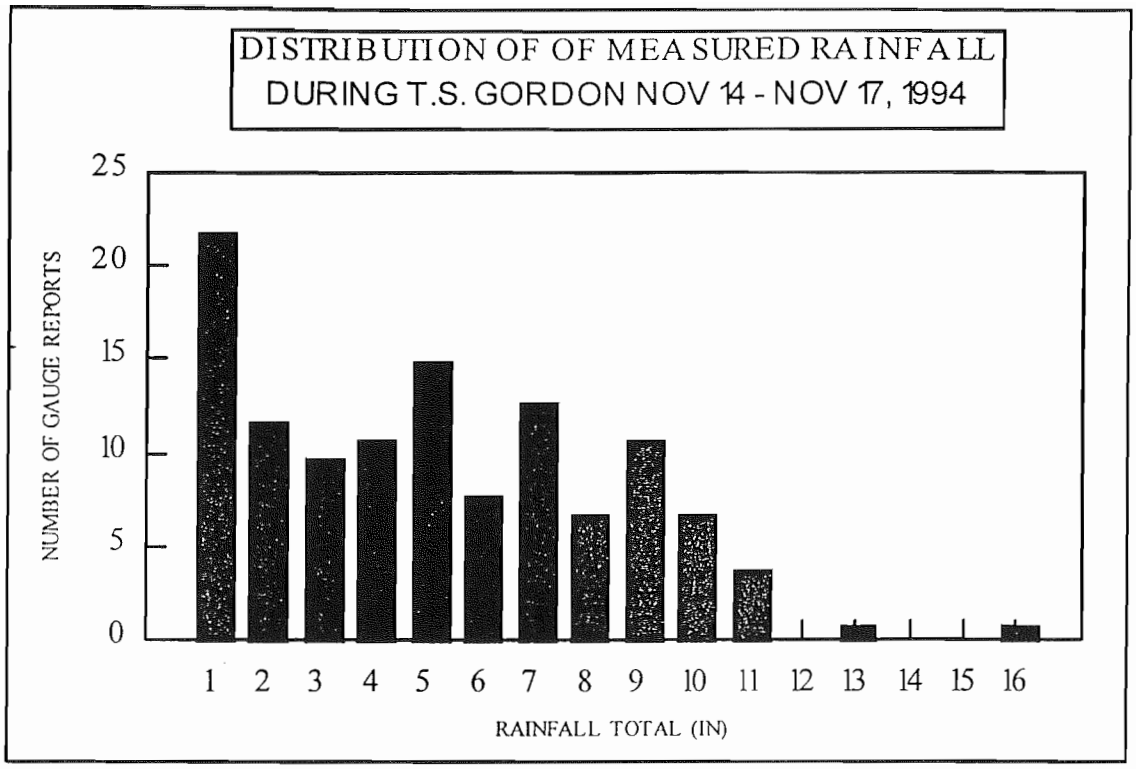


Figure 8 - Frequency distribution of measured rainfall totals.

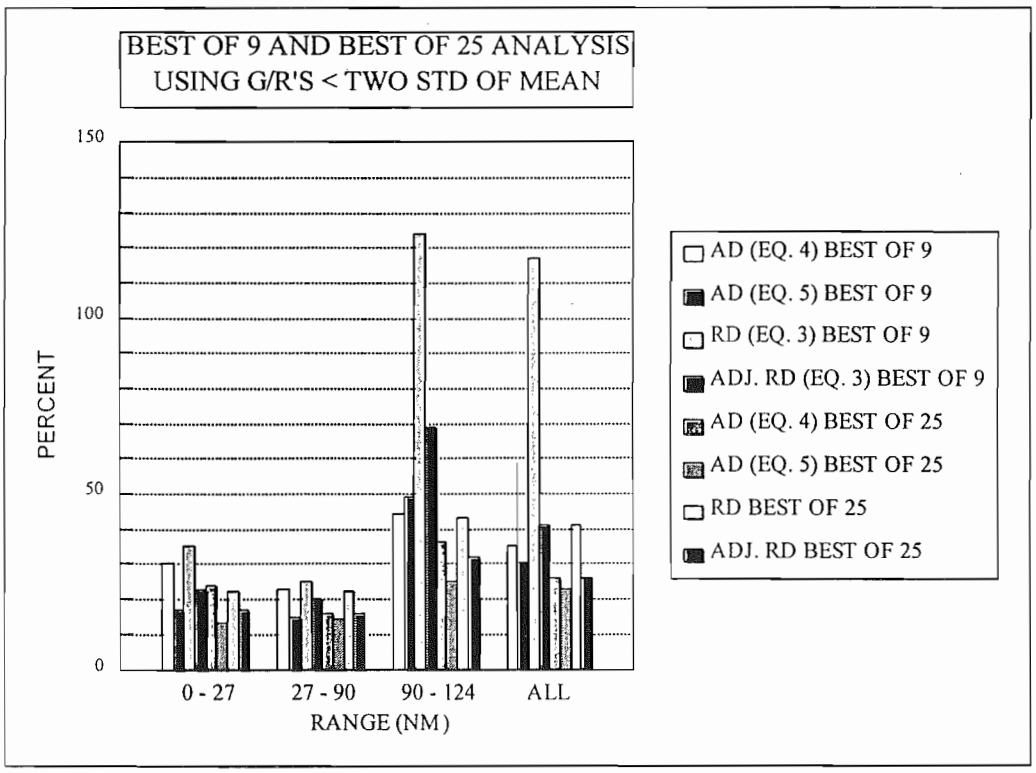


Figure 9 - Average Differences (AD) and Relative Dispersions (RD) comparison graph for the best of 9 and best of 25 bins.

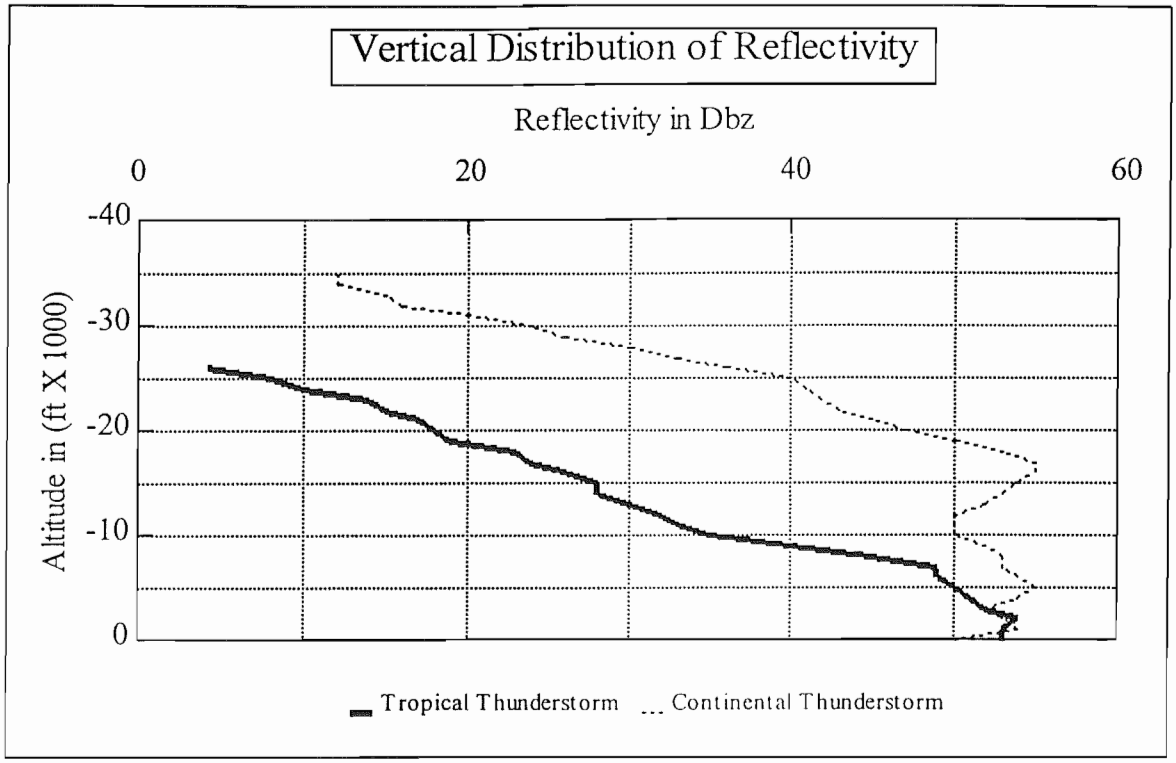


Figure 10 - Hypothetical graph of distribution of reflectivity in the vertical for tropical and non-tropical thunderstorms.

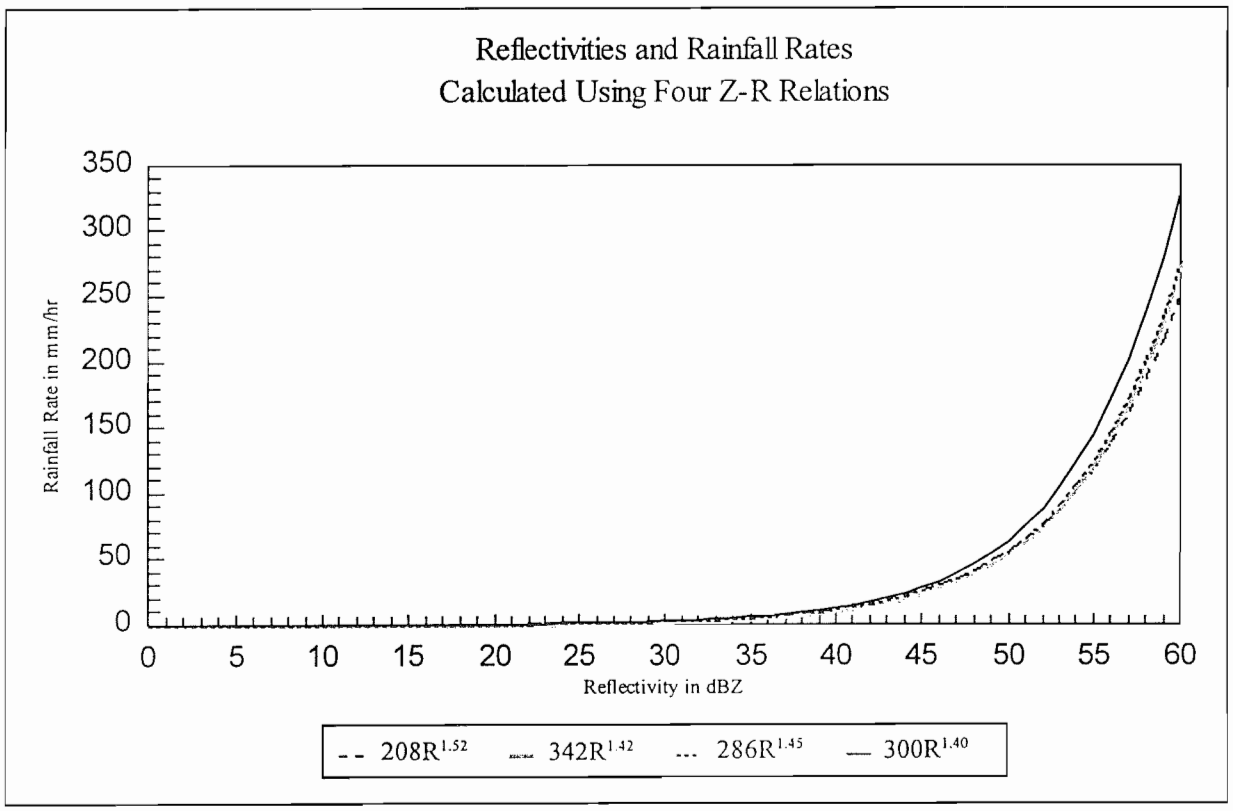


Figure 11 - Output using four different Z-R relations. The Z-Rs presented represent rainfall in various tropical environments along with the current default; $208R^{1.52}$ - Hawaii orographic rainfall (developed by Wexler, 1948), $342R^{1.42}$ Delhi, India, for non-orographic monsoon rains (developed by Ramana Murty and Gupta, 1959), $286R^{1.45}$ Miami, Florida, and $300R^{1.40}$ - currently employed by the WSR-88D (Marshall and Palmer).

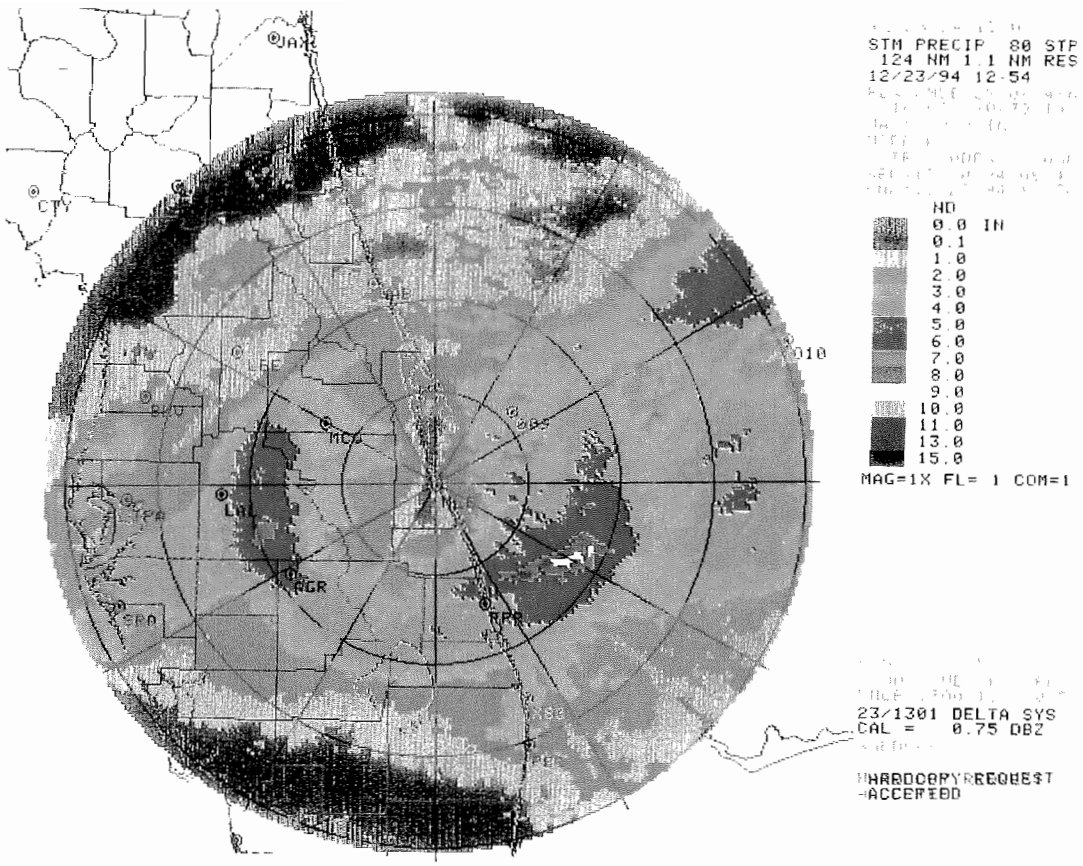


Plate 1 - The Storm Total Precipitation (STP) with range rings indicated every 30 nm. Note bright band between about 35 nm and 70 nm.

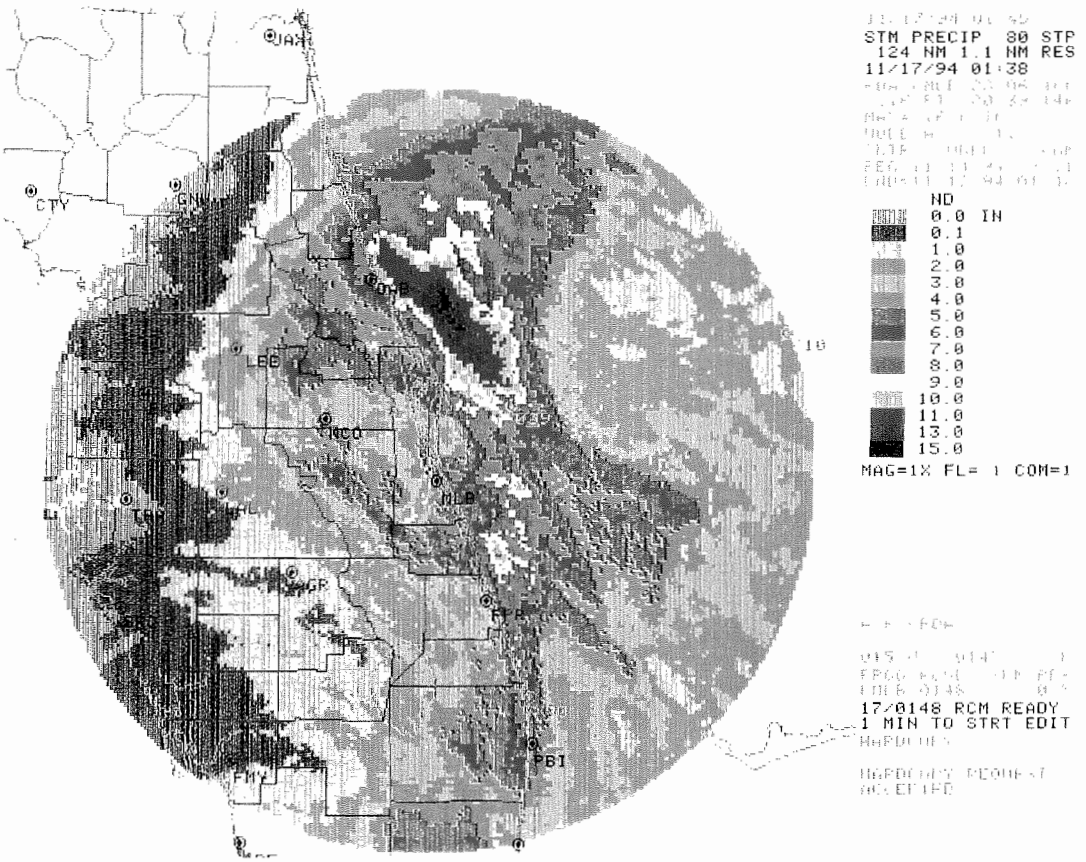


Plate 2 - Storm total precipitation product from the MLB WSR-88D radar for the time period from 1311 UTC on November 14, 1994, to 0410 UTC on November 17, 1994. Note sharp coastal transition with extreme rainfall indicated offshore.

# Appendix A

9 - BIN ANALYSIS

| PARAMETER | RANGES | CENTER | BEST | MAX | MINIMUM | AVERAGE |
|---|---|---|---|---|---|---|
| MEAN RADAR BIAS (EQ. 1) | ALL | 1.65 | 1.44 | 1.42 | 1.90 | 1.64 |
| MEAN RADAR BIAS (EQ. 2) | ALL | 2.58 | 1.88 | 1.88 | 3.14 | 2.52 |
| ADJ. (EQ. 2) | ALL | 2.05 | 1.57 | 1.57 | NC | 1.88 |
| REL. DISP. (EQ. 3) | ALL | 128% | 117% | 118% | NC | 132% |
| ADJ. (EQ. 3)* | ALL | 71% | 41% | 42% | NC | 44% |
| AVG. DIFF. (EQ. 4) | ALL | 48% | 37% | 41% | 55% | 48% |
| ADJ. AVG. DIFF. (EQ. 4)* | ALL | 46% | 35% | 39% | NC | 46% |
| AVG. DIFF. 2 (EQ. 5) | ALL | 76% | 46% | 54% | 86% | 72% |
| ADJ. AVG. DIFF. (EQ. 5)* | ALL | 49% | 30% | 37% | NC | 41% |
| MEAN RADAR BIAS (EQ. 1) | 0 - 27nm (0 - 52km) | 1.79 | 1.47 | 1.46 | 2.16 | 1.75 |
| MEAN RADAR BIAS (EQ. 2) | 0 - 27nm (0 - 52km) | 2.35 | 1.53 | 1.53 | 39.58 | 1.94 |
| ADJ. (EQ. 2)* | 0 - 27nm (0 - 52km) | 2.04 | 1.43 | 1.43 | 2.86 | 1.71 |
| REL. DISP. (EQ. 3) | 0 - 27nm (0 - 52km) | 81% | 35% | 36% | 416% | 46% |
| ADJ. (EQ. 3)* | 0 - 27nm (0 - 52km) | 65% | 23% | 24% | NC | 32% |
| AVG. DIFF. (EQ. 4) | 0 - 27nm (0 - 52km) | 44% | 32% | 33% | NC | 43% |
| ADJ. AVG. DIFF. (EQ. 4)* | 0 - 27nm (0 - 52km) | 42% | 30% | 30% | NC | 39% |
| AVG. DIFF. 2 (EQ. 5) | 0 - 27nm (0 - 52km) | 63% | 22% | 22% | NC | 38% |
| ADJ. AVG. DIFF. (EQ. 5)* | 0 - 27nm (0 - 52km) | 46% | 17% | 17% | NC | 29% |
| MEAN RADAR BIAS (EQ. 1) | 27 - 90 (52 - 173km) | 1.45 | 1.28 | 1.27 | 1.62 | 1.43 |
| MEAN RADAR BIAS (EQ. 2) | 27 - 90 (52 - 173km) | 1.57 | 1.33 | 1.32 | 1.82 | 1.53 |
| ADJ. (EQ. 2)* | 27 - 90 (52 - 173km) | 1.53 | 1.32 | 1.35 | 1.77 | 1.50 |
| REL. DISP. (EQ. 3) | 27 - 90 (52 - 173km) | 29% | 25% | 27% | 36% | 28% |
| ADJ. (EQ. 3)* | 27 - 90 (52 - 173km) | 24% | 20% | 19% | 24% | 23% |
| AVG. DIFF. (EQ. 4) | 27 - 90 (52 - 173km) | 44% | 31% | 37% | NC | 43% |
| ADJ. AVG. DIFF. (EQ. 4)* | 27 - 90 (52 - 173km) | 34% | 23% | 24% | NC | 32% |
| AVG. DIFF. 2 (EQ. 5) | 27 - 90 (52 - 173km) | 34% | 27% | 35% | NC | 32% |
| ADJ. AVG. DIFF. (EQ. 5)* | 27 - 90 (52 - 173km) | 16% | 15% | 17% | NC | 16% |
| MEAN RADAR BIAS (EQ. 1) | 90 - 124 nm (173 - 230 km) | 1.93 | 1.77 | 1.72 | 2.28 | 1.97 |
| MEAN RADAR BIAS (EQ. 2) | 90 - 124 nm (173 - 230 km) | 4.01 | 2.80 | 2.78 | 5.19 | 4.07 |
| ADJ. (EQ. 2)* | 90 - 124 nm (173 - 230 km) | 2.79 | 2.33 | 2.31 | 3.10 | 2.56 |
| REL. DISP. (EQ. 3) | 90 - 124 nm (173 - 230 km) | 125% | 124% | 125% | 152% | 125% |
| ADJ. (EQ. 3)* | 90 - 124 nm (173 - 230 km) | 80% | 69% | 70% | 45% | 64% |
| AVG. DIFF. (EQ. 4) | 90 - 124 nm (173 - 230 km) | 57% | 47% | 50% | NC | 58% |
| ADJ. AVG. DIFF. (EQ. 4)* | 90 - 124 nm (173 - 230 km) | 54% | 44% | 49% | NC | 54% |
| AVG. DIFF. 2 (EQ. 5) | 90 - 124 nm (173 - 230 km) | 104% | 65% | 73% | NC | 101% |
| ADJ. AVG. DIFF. (EQ. 5)* | 90 - 124 nm (173 - 230 km) | 53% | 49% | 50% | NC | 40% |

* - Re-calculated using G/R values which did'nt exceed the mean by greater than or equal to two standard deviations.

NC - Not Calculated

# Appendix B

25 - BIN ANALYSIS

| PARAMETER | RANGES | BEST | MAX | MIN |
|---|---|---|---|---|
| MEAN RADAR BIAS (EQ. 1) | ALL | 1.35 | 1.32 | 2.06 |
| MEAN RADAR BIAS (EQ. 2) | ALL | 1.47 | 1.45 | 5.65 |
| ADJ. (EQ. 2) | ALL | 1.36 | 1.35 | NC |
| REL. DISP. (EQ. 3) | ALL | 41% | 43% | NC |
| ADJ. (EQ. 3)* | ALL | 26% | 30% | NC |
| AVG. DIFF. (EQ. 4) | ALL | 29% | 36% | 58% |
| ADJ. AVG. DIFF. (EQ. 4)* | ALL | 26% | 35% | NC |
| AVG. DIFF. 2 (EQ. 5) | ALL | 28% | 39% | 183% |
| ADJ. AVG. DIFF. (EQ. 5)* | ALL | 23% | 34% | NC |
| MEAN RADAR BIAS (EQ. 1) | 0 - 27nm (0 - 52km) | 1.39 | 1.37 | 2.28 |
| MEAN RADAR BIAS (EQ. 2) | 0 - 27nm (0 - 52km) | 1.40 | 1.39 | 4.75 |
| ADJ. (EQ. 2)* | 0 - 27nm (0 - 52km) | 1.33 | 1.35 | 2.52 |
| REL. DISP. (EQ. 3) | 0 - 27nm (0 - 52km) | 22% | 23% | 209% |
| ADJ. (EQ. 3)* | 0 - 27nm (0 - 52km) | 17% | 15% | 75% |
| AVG. DIFF. (EQ. 4) | 0 - 27nm (0 - 52km) | 27% | 28% | NC |
| ADJ. AVG. DIFF. (EQ. 4)* | 0 - 27nm (0 - 52km) | 24% | 25% | NC |
| AVG. DIFF. 2 (EQ. 5) | 0 - 27nm (0 - 52km) | 16% | 18% | NC |
| ADJ. AVG. DIFF. (EQ. 5)* | 0 - 27nm (0 - 52km) | 13% | 11% | NC |
| MEAN RADAR BIAS (EQ. 1) | 27 - 90 (52 - 173km) | 1.19 | 1.16 | 1.76 |
| MEAN RADAR BIAS (EQ. 2) | 27 - 90 (52 - 173km) | 1.21 | 1.19 | 2.04 |
| ADJ. (EQ. 2)* | 27 - 90 (52 - 173km) | 1.21 | 1.20 | 1.93 |
| REL. DISP. (EQ. 3) | 27 - 90 (52 - 173km) | 22% | 26% | 40% |
| ADJ. (EQ. 3)* | 27 - 90 (52 - 173km) | 16% | 17% | 29% |
| AVG. DIFF. (EQ. 4) | 27 - 90 (52 - 173km) | 22% | 35% | NC |
| ADJ. AVG. DIFF. (EQ. 4)* | 27 - 90 (52 - 173km) | 16% | 18% | NC |
| AVG. DIFF. 2 (EQ. 5) | 27 - 90 (52 - 173km) | 21% | 36% | NC |
| ADJ. AVG. DIFF. (EQ. 5)* | 27 - 90 (52 - 173km) | 14% | 15% | NC |
| MEAN RADAR BIAS (EQ. 1) | 90 - 124 nm (173 - 230 km) | 1.64 | 1.59 | 2.48 |
| MEAN RADAR BIAS (EQ. 2) | 90 - 124 nm (173 - 230 km) | 1.84 | 1.81 | 11.11 |
| ADJ. (EQ. 2)* | 90 - 124 nm (173 - 230 km) | 1.71 | 1.68 | 5.39 |
| REL. DISP. (EQ. 3) | 90 - 124 nm (173 - 230 km) | 43% | 46% | 257% |
| ADJ. (EQ. 3)* | 90 - 124 nm (173 - 230 km) | 32% | 35% | 140% |
| AVG. DIFF. (EQ. 4) | 90 - 124 nm (173 - 230 km) | 40% | 42% | NC |
| ADJ. AVG. DIFF. (EQ. 4)* | 90 - 124 nm (173 - 230 km) | 36% | 41% | NC |
| AVG. DIFF. 2 (EQ. 5) | 90 - 124 nm (173 - 230 km) | 31% | 38% | NC |
| ADJ. AVG. DIFF. (EQ. 5)* | 90 - 124 nm (173 - 230 km) | 25% | 32% | NC |

* - Re-calculated using G/R values which did'nt exceed the mean by greater than or equal to two standard deviations.
NC - Not Calculated